Edge-state-induced Andreev oscillation in quantum anomalous Hall insulator-superconductor junctions

Biao Lian, Jing Wang, and Shou-Cheng Zhang

Phys. Rev. B **93**, 161401 — Published 7 April 2016

DOI: 10.1103/PhysRevB.93.161401

Edge State Induced Andreev Oscillation in Quantum Anomalous Hall Insulator-Superconductor Junctions

Biao Lian,[1] Jing Wang,[2,1,3] and Shou-Cheng Zhang[1,3]

[1] *Department of Physics, McCullough Building, Stanford University, Stanford, California 94305-4045, USA*
[2] *State Key Laboratory of Surface Physics and Department of Physics, Fudan University, Shanghai 200433, China*
[3] *Stanford Institute for Materials and Energy Sciences, SLAC National Accelerator Laboratory, Menlo Park, California 94025, USA*

(Dated: March 23, 2016)

We study the quantum Andreev oscillation induced by interference of the edge chiral Majorana fermions in junctions made of quantum anomalous Hall (QAH) insulators and superconductors (SCs). We show two chiral Majorana fermions on a QAH edge with SC proximity generically have a momentum difference Δk, which depends on the chemical potentials of both the QAH insulator and the SC. Due to the spatial interference induced by Δk, the longitudinal conductance of QAH-SC junctions oscillates with respect to the edge lengths and the chemical potentials, which can be probed via charge transport. Furthermore, we show the dynamical SC phase fluctuation will give rise to a geometrical correction to the longitudinal conductance of the junctions.

PACS numbers: 73.20.-r 73.40.Cg 74.45.+c

Quantum anomalous Hall (QAH) state is known as a two-dimensional (2D) topological state which has an integer number N_h of chiral fermions at the edge and exhibits a quantized Hall conductance in the absence of an external magnetic field[1–11]. For non-interacting fermionic systems, N_h is the total Chern number of the occupied electronic bands. The QAH state with $N_h = 1$ has been experimentally realized in both Cr-doped[12–15] and V-doped[16] $(Bi,Sb)_2Te_3$ magnetic topological insulator thin films. When the QAH state is proximity-coupled with a normal s-wave superconductor (SC), the system becomes a chiral topological SC (TSC) and the edge chiral Majorana fermions arise[17–22]. Such systems may exhibit exotic transport phenomena due to the existence of electrically neutral Majorana edge states[23–30]. However, not much effort has been made to understand how exactly the electric current flows from a QAH insulator into an adjacent normal SC (or TSC), both of which are conductive and dissipationless. This is crucial to the study of coupled QAH/SC transport experiments.

In this Letter, we show the conductance of a QAH/SC junction exhibits an Andreev oscillation due to the interference of the chiral Majorana fermions on the QAH edge proximity-coupled to the SC. Such an interference is induced by the momentum difference Δk between the two chiral Majorana fermions on the same edge, which can be tuned by the chemical potentials of both the QAH insulator and the SC. As a result, the two-terminal longitudinal conductance of the QAH/SC junction oscillates with respect to the length of the proximity-coupled edge and the chemical potentials of QAH and SC, while the Hall conductance is quantized. Similar Andreev oscillation in the longitudinal conductance occurs for the other junctions of QAH insulator and SC shown in Fig. 3, while the Hall conductance always remains quantized. Furthermore, we consider the QAH/TSC/QAH junction, where there is only a single chiral Majorana fermion on each superconducting edge. The dynamical phase fluctuation of SC will have a $1/d_{\rm SC}^3$ geometric correction to the previously predicted half-quantized longitudinal conductance $e^2/2h$[25,28], where $d_{\rm SC}$ is the size of TSC in the junction, e is the electron charge and h is the Plank constant. All the conclusions discussed here also hold for integer quantum Hall (IQH) insulator/SC junctions.

The basic mechanism of the edge chiral Majorana fermions interference in a QAH/SC junction can be easily understood in the geometry shown in Fig. 1(a), where a QAH insulator and a normal SC (NSC) are attached into a y-direction translational invariant cylinder. Since a QAH with Chern number N_h is topologically equivalent to a chiral TSC with Bogoliubov-de Gennes (BdG) Chern number $N = 2N_h$, the N_h chiral fermions on the QAH edge will become $2N_h$ chiral Majorana fermions under the proximity effect of the NSC. For simplicity, we restrict ourselves to QAH with $N_h = 1$. In this case, the two chiral Majorana fermions on the same QAH edge are related to each other by the particle-hole symmetry (PHS). In general, the energy dispersions of these two chiral Majorana fermions will not coincide with each other. To show this, we take the two-band lattice Hamiltonian for the QAH:

$$\mathcal{H}_{\rm QAH} = \sum_{\mathbf{k}} c_{\mathbf{k}}^\dagger \left[\boldsymbol{\zeta}(\mathbf{k})\cdot\boldsymbol{\sigma} - \mu_h\right] c_{\mathbf{k}} \ , \tag{1}$$

and the s-wave BdG Hamiltonian for the NSC:

$$\mathcal{H}_{\rm NSC} = \sum_{\mathbf{k}} c_{\mathbf{k}}^\dagger \left[\epsilon(\mathbf{k}) - \mu_s\right] c_{\mathbf{k}} + (\Delta_s c_{\mathbf{k}}^T i\sigma_y c_{-\mathbf{k}} + \text{H.c.}) \ . \tag{2}$$

Here, the basis $c_{\mathbf{k}} = (c_{\mathbf{k}\uparrow}, c_{\mathbf{k}\downarrow})^T$, $\boldsymbol{\zeta}(\mathbf{k}) = (M - B(\cos k_x a + \cos k_y a), A\sin k_x a, A\sin k_y a)$, $\boldsymbol{\sigma} = (\sigma_x, \sigma_y, \sigma_z)$ are the Pauli matrices, $\epsilon(\mathbf{k}) = B(2 - \cos k_x a - \cos k_y a)$ is the kinetic energy, μ_h and μ_s are the chemical potentials of the QAH and the NSC, respectively, a is the lattice constant, and Δ_s is the pairing amplitude. The QAH insulator is realized in the regime $|M| < 2|B|$ and $|\mu_h| < 2|B| - |M|$.

In Fig. 1(b), the BdG spectrum of the cylinder is calculated as a function of k_y with parameters $a = 0.8$, $B = 1.5625$, $M = 2.625$, $A = 1.25$, $\Delta_s = 0.3$, $\mu_h = 0.2$ and $\mu_s = 0.5$. The distinction between the dispersions of two chiral Majorana fermions ψ_1 and ψ_2 on the same edge is clearly seen, where the momentum difference between ψ_1 and ψ_2 at zero energy is denoted as Δk.

Now we consider a QAH/NSC junction as shown in Fig. 1(c), where the length of the QAH edge (the right edge) in contact with NSC is $d_{\rm SC}$. The low energy physics in the QAH is dominated by the gapless edge electrons. When an edge electron denoted by $\bar{c}_k$ in the lower edge enters into the right edge of the QAH, it splits into two chiral Majorana fermions ψ_1 and ψ_2. Whenever ψ_1 and ψ_2 have a momentum difference Δk, a phase difference $\phi = \Delta k d_{\rm SC}$ will be accumulated between them after propagating along the edge of length $d_{\rm SC}$. For $\phi \neq 2m\pi$ ($m \in \mathbb{Z}$), the outgoing state in the upper edge will become a superposition of electron and hole $u\bar{c}_k + v\bar{c}^\dagger_k$, where $|u|^2 + |v|^2 = 1$ due to the unitarity. Therefore, an incident electron from the lower QAH edge has a probability $|v|^2$ turning into a hole at the upper QAH edge, which is denoted as the Andreev reflection probability $R_A = |v|^2$. Accordingly, the normal reflection probability is $R = |u|^2 = 1 - R_A$. R_A can be calculated by solving a 2D Shrödinger equation numerically[31]. Here we give an approximate expression for R_A via a simplified picture as follows. Due to the PHS, the two edge chiral Majorana modes $\psi_{1,2}$ at zero energy take the generic form

$$\psi_1 = \alpha \bar{c}_{\frac{\Delta k}{2}} + \beta \bar{c}^\dagger_{-\frac{\Delta k}{2}} , \quad \psi_2 = \beta^* \bar{c}_{-\frac{\Delta k}{2}} + \alpha^* \bar{c}^\dagger_{\frac{\Delta k}{2}} , \quad (3)$$

where $|\alpha|^2 + |\beta|^2 = 1$, while $\bar{c}_k$ and $\bar{c}^\dagger_k$ are the edge electron annihilation and creation operators, respectively. When $\Delta_s = 0$, we recover the QAH edge state and get $\alpha = 1$, $\beta = 0$. For convenience the QAH edge is parameterized as ℓ, where the origin $\ell = 0$ is set at the lower right corner of QAH. The chiral edge mode for an incident electron with momentum k_I is then $\Psi(\ell) = \bar{c}_{k_I} = \bar{c}(\ell) e^{ik_I \ell}$ on the lower edge $\ell < 0$, and $\Psi(\ell) = u\bar{c}(\ell) e^{ik_I \ell} + v\bar{c}^\dagger(\ell) e^{-ik_I \ell}$ on the upper edge $\ell > d_{\rm SC}$. The vanishing hole probability at $\ell = 0$ requires $\Psi(\ell) = \mathcal{N}[\alpha^* \psi_1(\ell) - \beta \psi_2(\ell)]$ on the right edge $0 < \ell < d_{SC}$, where $\mathcal{N}$ is a normalization factor. The continuity condition for $\Psi(\ell)$ at $\ell = d_{\rm SC}$ of junction is $\Psi(d^+_{SC}) \propto \Psi(d^-_{SC})$, then the Andreev reflection probability $R_A = |v|^2$ is found to be[31]:

$$R_A(\phi) = \frac{4|\alpha\beta|^2 \sin^2(\phi/2)}{(|\alpha^2| - |\beta^2|)^2 + 8|\alpha\beta|^2 \sin^2(\phi/2)} , \quad (4)$$

with $\phi = \Delta k d_{\rm SC}$. From Eq. (4), firstly, R_A oscillates as a function of $d_{\rm SC}$ with a period $2\pi/\Delta k$. Secondly, $0 \leq R_A \leq 1/2$, which agrees well with the numerical results shown later. For an illustration, R_A and R are plotted with respect to $d_{\rm SC}$ for $|\alpha|^2 = 1 - |\beta|^2 = 0.7$ in Fig. 1(d) based on Eq. (4).

Physically, due to the charge conservation, such a process must have a Cooper pair created and injected into the NSC with a probability R_A[32,33]. The junction therefore has a nonzero conductance when a current I is applied between leads 1 and 3 as shown in Fig. 1(c). We employ the Landauer-Büttiker formula $I_i = (e^2/h) \sum_j (T_{ij} V_j - T_{ji} V_i)$ to calculate the conductance, where I_i is the current flowing out of lead i, V_i is the voltage of lead i, and T_{ij} is the generalized transmission probability from lead i to lead j contributed by both the normal scattering and the Andreev scattering[33]. In this 4-terminal junction, $T_{43} = T_{32} = 2R_A = t$ represents the charge transmitted between QAH and NSC, $T_{42} = 1 - 2R_A = r$ is the charge reflected from lead 4 to 2[34], $T_{14} = T_{21} = 1$, and all the other T_{ij} are zero. One finds

$$\sigma_{13} = \frac{I}{V_1 - V_3} = 2R_A \frac{e^2}{h} , \quad \sigma_{24} = \frac{I}{V_2 - V_4} = \frac{e^2}{h} . \quad (5)$$

Therefore, the two-terminal longitudinal conductance σ_{13} exhibits an Andreev oscillation with respect to ϕ, while the Hall conductance σ_{24} remains quantized.

In order to observe the oscillatory σ_{13}, one needs to tune the phase difference ϕ. One way is to continuously tune the length $d_{\rm SC}$ of NSC in contact with QAH, which is not quite feasible in experiments. The other way is to tune the momentum difference Δk, which can be achieved by tuning the chemical potential of either the QAH or the NSC. Since states ψ_1 and ψ_2 form a PHS pair, their dispersions will shift oppositely in energy (up and down, respectively) as the chemical potential varies, which results in a change of Δk. To verify this argument, we have calculated Δk numerically as a function of μ_h and μ_s for the model and parameters mentioned above,

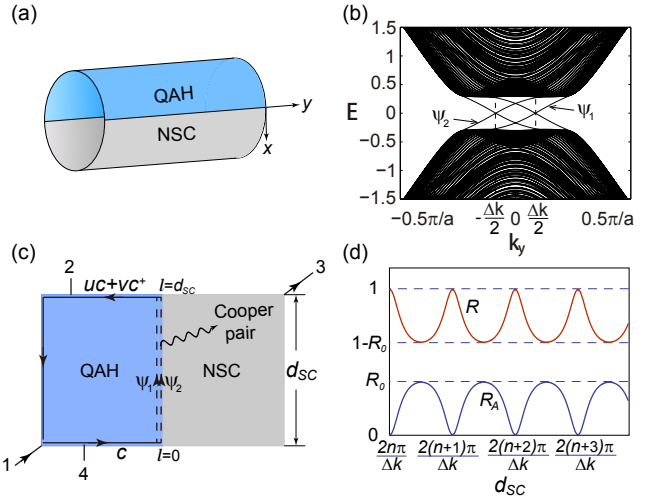

FIG. 1. (color online). (a) The QAH/NSC junction in cylinder geometry. (b) The BdG spectrum of the junction in (a), where the two chiral Majorana modes have a momentum difference Δk. (c) Illustration of a QAH/NSC junction with an edge length $d_{\rm SC}$. (d) The Andreev reflection probability R_A and the normal reflection probability R of the junction with respect to $d_{\rm SC}$.

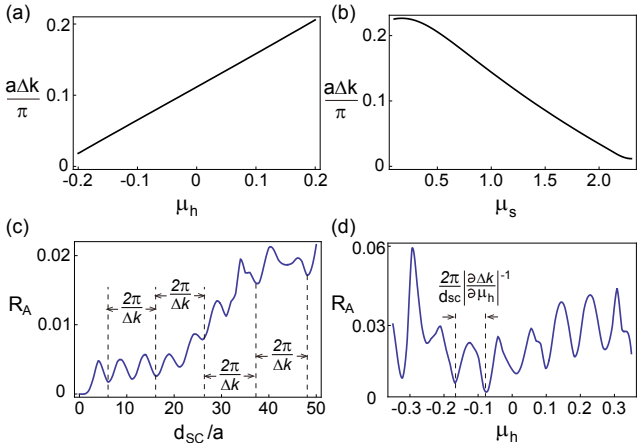

FIG. 2. (color online). (a) Δk as a function of μ_h with $\mu_s = 0.5$. (b) Δk as a function of μ_s with $\mu_h = 0.2$. (c) R_A of an edge electron wave packet with respect to $d_{\rm SC}$ calculated for $(\mu_h, \mu_s) = (0.2, 0.8)$. (d) R_A of an edge electron wave packet with respect to μ_h calculated for $\mu_s = 0.8$ and $d_{\rm SC} = 50a$.

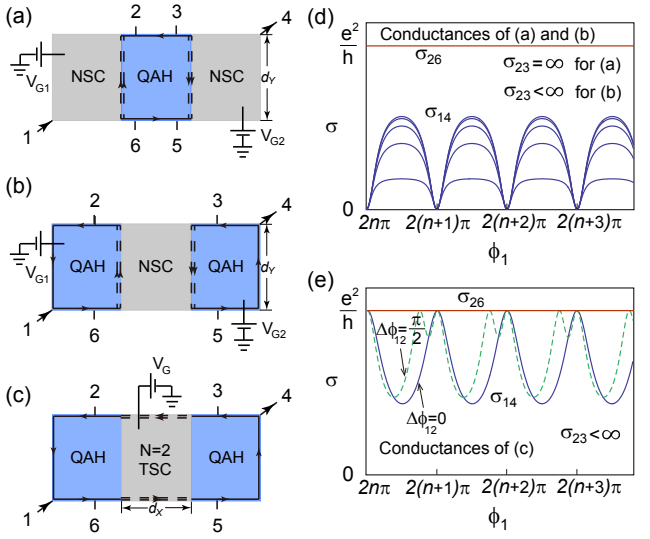

FIG. 3. (color online). (a)-(c) Illustration of three examples of 6-terminal QAH/SC junctions. (d) σ_{14} and σ_{26} of junctions (a) and (b) (which are the same) with respect to ϕ_1 for $\phi_2 = n\pi/5 (\mathrm{mod}\ 2\pi)$ ($1 \le n \le 5$ from lower to higher). Note their σ_{23} are different. (e) σ_{14} and σ_{26} of junction (c) vs. ϕ_1 for $\Delta\phi_{12} = 0, \pi/2$, respectively.

which are presented in Fig. 2(a) ($\mu_s = 0.5$) and Fig. 2(b) ($\mu_h = 0.2$), respectively. The results show Δk depends almost linearly on μ_h and μ_s. Thus, one should be able to observe the conductance oscillation by tuning μ_h or μ_s. As a numerical check, we further calculated the real space evolution of an edge electron wave packet in a low energy window $E \in [-0.1, 0.1]$ from lead 4 to 2 in the junction, where we chose a lattice size 30×50 for the QAH side and $18 \times L$ for the NSC side with $0 \le L \le 50$, and adopted a sine-square deformation to reduce the finite size effect[31,35,36]. The contact edge length $d_{\rm SC} \equiv La$. Fig. 2(c) shows R_A as a function of $d_{\rm SC}$ for $(\mu_h, \mu_s) = (0.2, 0.8)$, where one finds the fundamental oscillation period of $2\pi/\Delta k \approx 11a$. We note the R_A oscillation does not reach zero and varies in the amplitude, because Δk is dispersive in the energy window of the wave packet. We further plot R_A vs. μ_h for $\mu_s = 0.8$ and $d_{\rm SC} = 50a$ in Fig. 2(d), where again one can identify the predicted oscillation period $(2\pi/d_{SC})|\partial\Delta k/\partial\mu_h|^{-1} \approx 0.08$. As shown in the supplementary material[31], the oscillation in R_A is robust against disorders. The only difference is that Δk will acquire a spatial dependence under disorders, and the phase difference ϕ will become $\phi = \int_0^{d_{\rm SC}} \Delta k \mathrm{d}\ell$.

In realistic QAH materials like magnetic $(\mathrm{Bi,Sb})_2\mathrm{Te}_3$ and graphene, Δk usually does not exceed $0.1\pi/a$ with a being the lattice constant. Thus, the spatial oscillation period in $d_{\rm SC}$ is usually between $10a$ and $10^2 a$. The slope $|\partial\Delta k/\partial\mu_h| \sim v_F^{-1} \sim 0.5\ (\mathrm{eV{\cdot}\AA})^{-1}$ with v_F the Fermi velocity of the QAH edge state, and $|\partial\Delta k/\partial\mu_s| \sim 0.1|\partial\Delta k/\partial\mu_h|$ is smaller according to our numerical results above. If we take a contact edge length $d_{\rm SC} = 1\ \mu$m and tune μ_h and μ_s, the oscillation periods of μ_h and μ_s will be of order of 1 meV and 10 meV respectively, in the accessible range of transport experiments. Due to the dispersion of Δk in energy, the oscillations become decoherent and invisible above a temperature scale $k_B T \equiv [2\pi/(d_{\rm SC}|\partial v_F^{-1}/\partial\mu_h|)]^{1/2}$. Typical values of $|\partial v_F^{-1}/\partial\mu_h| \sim 0.5\ \mathrm{eV}^{-2}\mathrm{\AA}^{-1}$ and $d_{\rm SC} = 1\mu$m would require $T < 300$ K, which is feasible in experiments.

All the above analysis of Majorana fermion interference can be generalized to other QAH/SC junctions. Fig. 3(a)-(c) shows three examples of 6-terminal junctions, each of which have two QAH edges proximity-coupled to SC. The chiral Majorana fermions (dashed lines) on these two edges (left and right in junctions (a) and (b), upper and lower in junction (c)) may have distinct phase differences ϕ_1 and ϕ_2, and therefore distinct Andreev reflection probabilities $R_{A1} = R_A(\phi_1)$ and $R_{A2} = R_A(\phi_2)$. Junctions (a) and (b) can be implemented by attaching QAH and NSC samples together, while the $N = 2$ TSC in junction (c) can be realized via SC proximity on top of the middle region of a QAH sample[28]. With a current I flowing between leads 1 and 4, the conductances $\sigma_{ij} = I/(V_i - V_j)$ can be similarly derived from the Landauer-Büttiker formula[31], as listed in Table I. The Hall conductance σ_{26} is quantized for all the three junctions. In particular, we note that junction (a), which is just the QAH system in a standard Hall bar with SC leads[37], has no difference in σ_{26} and σ_{23} with the Hall bar with metallic leads. However, σ_{14} of such a junction with SC leads is oscillatory with ϕ_1 and ϕ_2. In junctions (a) and (b), ϕ_1 and ϕ_2 can be tuned independently by the gate voltages V_{G1} and V_{G2}, respectively. The blue curves in Fig. 3(d) show σ_{14} vs. ϕ_1 for fixed $\phi_2 = n\pi/5 (\mathrm{mod}\ 2\pi)$ ($1 \le n \le 5$) and $|\alpha|^2 = 0.7$. In junction (c), ϕ_1 and ϕ_2 can be tuned together by the gate

TABLE I. The conductances of junctions (a)-(c) shown in Fig. 3 calculated by the Landauer-Büttiker formula.

Junction	σ_{14}	σ_{23}	σ_{26}
(a)	$\frac{2R_{A1}R_{A2}}{R_{A1}+R_{A2}-2R_{A1}R_{A2}}\frac{e^2}{h}$	∞	$\frac{e^2}{h}$
(b)	$\frac{2R_{A1}R_{A2}}{R_{A1}+R_{A2}-2R_{A1}R_{A2}}\frac{e^2}{h}$	$\frac{2R_{A1}R_{A2}}{R_{A1}+R_{A2}-4R_{A1}R_{A2}}\frac{e^2}{h}$	$\frac{e^2}{h}$
(c)	$\frac{R_{A1}+R_{A2}-4R_{A1}R_{A2}}{R_{A1}+R_{A2}-2R_{A1}R_{A2}}\frac{e^2}{h}$	$\frac{R_{A1}+R_{A2}-4R_{A1}R_{A2}}{2R_{A1}R_{A2}}\frac{e^2}{h}$	$\frac{e^2}{h}$

voltage V_G, with $\Delta\phi_{12} \equiv \phi_1 - \phi_2$ approximately fixed. In this case, $\sigma_{14}(\phi_1)$ for $\Delta\phi_{12} = 0$ and $\pi/2$ are shown in Fig. 3(e).

Finally, we discuss the QAH/TSC/QAH junction as shown in Fig. 4, where the TSC has only a single chiral Majorana state ψ_i $(1 \le i \le 4)$ on the i-th edge. At the BdG level, an electron incident from lead 1 will split into ψ_1 which is totally reflected and ψ_2 which is perfectly transmitted to lead 2, resulting in a half quantized longitudinal conductance $\sigma_{12} = e^2/2h$[25,28]. Here we show when the dynamical fluctuation of the SC phase θ is considered, σ_{12} is no longer exactly quantized but has a geometry-dependent correction $\delta\sigma_{12}$. Such dynamics of the 2D TSC can be described by the effective Hamiltonian[31]

$$H_{\rm eff} = \frac{1}{2g}\int_{\mathcal{M}_{\rm sc}} \mathrm{d}^2\mathbf{x}\left[(\partial_t\theta)^2 + v_s^2(\nabla\theta)^2\right]$$
$$-iv_F\sum_{i=1}^{4}\left[(\psi_i\psi_{i+1}\mathbf{n}_i\cdot\nabla\theta)_{\mathbf{x}_i} + \int_{\partial_i\mathcal{M}_{\rm sc}}\mathrm{d}\ell\psi_i\partial_\ell\psi_i\right], \quad (6)$$

where $\psi_5 \equiv -\psi_1$, $\mathcal{M}_{\rm sc}$ and $\partial_i\mathcal{M}_{\rm sc}$ are the bulk and i-th edge of the TSC, and the vector potential $\mathbf{A} = 0$ gauge is chosen. The Ginzburg-Landau theory gives $g = \mu_0\hbar^2/16m^2\xi^4 w B_c^2$ and $v_s = \hbar/4m\xi$, where μ_0 is the vacuum permeability, m is the electron effective mass, ξ is the coherence length, B_c is the critical magnetic field[38], and w is the thickness of the TSC[39]. The vector $\mathbf{n}_i$ shown in Fig. 4 characterizes the interaction between Majorana fermions ψ_i and the supercurrent $\mathbf{j}_s \propto \nabla\theta$ at $\mathbf{x}_i$, and $|\mathbf{n}_i|$ is of the order of the Majorana edge state width. As a result, ψ_1 (ψ_2) will have a nonzero scattering amplitude into ψ_3 (ψ_4) via $\mathbf{j}_s$ (wavy lines in Fig. 4), leading to a correction to the longitudinal conductance[31]

$$\delta\sigma_{12} \equiv \sigma_{12} - \frac{e^2}{2h} = \frac{e^2}{2h}\frac{g\hbar}{16\pi^2 v_s}\sum_{p,q\in\mathbb{Z}} f(p\mathbf{d}_X + q\mathbf{d}_Y), \quad (7)$$

where $\mathbf{d}_{X,Y}$ are vectors along the TSC edges as shown in Fig. 4. The function $f(\mathbf{x})$ is given by

$$f(\mathbf{x}) = \sum_{i,j=1}^{4}(\mathbf{n}_i\cdot\nabla)(\mathbf{n}_j\cdot\nabla)\frac{(-1)^{i-j}(1-\delta_{ij})}{\sqrt{|\mathbf{x}-\mathbf{t}_{ij}|^2 + v_s^2|\mathbf{t}_{ij}|^2/v_F^2}},$$

where $\mathbf{t}_{ij}$ equals $\mathbf{d}_X/2$ for $i-j$ odd and $\mathbf{d}_Y/2$ for $i-j$ even. Therefore, $\delta\sigma_{12}$ depends on the aspect ratio $\tau = d_Y/d_X$ of the TSC, and scales as $1/d_X^3$ for a fixed τ. In particular, $\delta\sigma_{12} > 0$ for $\tau \gg 1$, and $\delta\sigma_{12} < 0$ for $\tau \ll 1$. For a 2D TSC with $w = 5$ nm, $\xi = 10$ nm, $B_c = 0.01$ T and an edge state width 10 nm, one has $|\delta\sigma_{12}| \sim 10^{-6}(e^2/h)$ for $d_{X,Y} \sim 1$ μm. Therefore, this geometric correction is generically small in experiments.

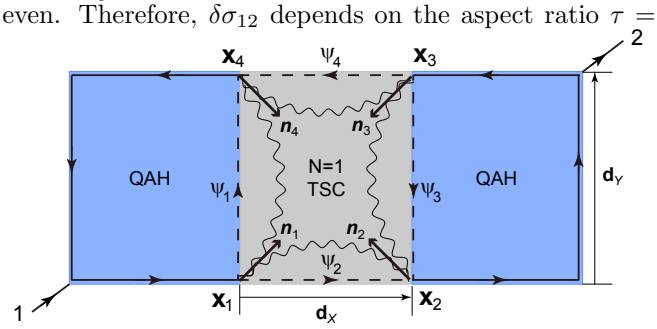

FIG. 4. Illustration of the QAH/TSC/QAH junction. The fluctuating supercurrent (the wavy lines) contributes a geometry-dependent correction to the conductance σ_{12}.

To conclude, we have proposed transport experiments to detect the Andreev oscillation due to the edge chiral Majorana fermion interference in the QAH/SC junctions. We emphasize that all the conclusions here also apply to ordinary IQH/SC junctions, provided the magnetic field realizing the IQH state is smaller than the upper critical field of the SC. Candidate materials include graphene and Niobium. Moreover, the longitudinal conductance may have multiple oscillation periods if the IQH (QAH) insulator has $N_h > 1$ edge chiral fermions, which remains to be studied in details in the future.

ACKNOWLEDGMENTS

We are grateful to Philip Kim for helpful discussions. This work is supported by the US Department of Energy, Office of Basic Energy Sciences, Division of Materials Sciences and Engineering, under Contract No. DE-AC02-76SF00515 and in part by the NSF under grant No. DMR-1305677. J.W. is supported by the National Thousand-Young-Talents Program.

[1] F. D. M. Haldane, Phys. Rev. Lett. **61**, 2015 (1988).
[2] C.-X. Liu, X.-L. Qi, X. Dai, Z. Fang, and S.-C. Zhang, Phys. Rev. Lett. **101**, 146802 (2008).
[3] X.-L. Qi, T. L. Hughes, and S.-C. Zhang, Phys. Rev. B **78**, 195424 (2008).
[4] M. Z. Hasan and C. L. Kane, Rev. Mod. Phys. **82**, 3045

(2010).
[5] X.-L. Qi and S.-C. Zhang, Rev. Mod. Phys. **83**, 1057 (2011).
[6] R. Yu, W. Zhang, H.-J. Zhang, S.-C. Zhang, X. Dai, and Z. Fang, Science **329**, 61 (2010).
[7] J. Wang, B. Lian, H. Zhang, Y. Xu, and S.-C. Zhang, Phys. Rev. Lett. **111**, 136801 (2013).
[8] M. Onoda and N. Nagaosa, Phys. Rev. Lett. **90**, 206601 (2003).
[9] J. Wang, B. Lian, H. Zhang, and S.-C. Zhang, Phys. Rev. Lett. **111**, 086803 (2013).
[10] J. Wang, B. Lian, and S.-C. Zhang, Phys. Scr. **T164**, 014003 (2015).
[11] C.-X. Liu, S.-C. Zhang, and X.-L. Qi, arXiv: 1508.07106.
[12] C.-Z. Chang, J. Zhang, X. Feng, J. Shen, Z. Zhang, M. Guo, K. Li, Y. Ou, P. Wei, L.-L. Wang, Z.-Q. Ji, Y. Feng, S. Ji, X. Chen, J. Jia, X. Dai, Z. Fang, S.-C. Zhang, K. He, Y. Wang, L. Lu, X.-C. Ma, and Q.-K. Xue, Science **340**, 167 (2013).
[13] X. Kou, S.-T. Guo, Y. Fan, L. Pan, M. Lang, Y. Jiang, Q. Shao, T. Nie, K. Murata, J. Tang, Y. Wang, L. He, T.-K. Lee, W.-L. Lee, and K. L. Wang, Phys. Rev. Lett. **113**, 137201 (2014).
[14] J. G. Checkelsky, R. Yoshimi, A. Tsukazaki, K. S. Takahashi, Y. Kozuka, J. Falson, M. Kawasaki, and Y. Tokura, Nat. Phys. **10**, 731 (2014).
[15] A. J. Bestwick, E. J. Fox, X. Kou, L. Pan, K. L. Wang, and D. Goldhaber-Gordon, Phys. Rev. Lett. **114**, 187201 (2015).
[16] C.-Z. Chang, W. Zhao, D. Y. Kim, H. Zhang, B. A. Assaf, D. Heiman, S.-C. Zhang, C. Liu, M. H. W. Chan, and J. S. Moodera, Nat. Mater. **14**, 473 (2015).
[17] A. P. Schnyder, S. Ryu, A. Furusaki, and A. W. W. Ludwig, Phys. Rev. B **78**, 195125 (2008).
[18] L. Fu and C. L. Kane, Phys. Rev. Lett. **100**, 096407 (2008).
[19] J. D. Sau, R. M. Lutchyn, S. Tewari, and S. Das Sarma, Phys. Rev. Lett. **104**, 040502 (2010).
[20] J. Alicea, Phys. Rev. B **81**, 125318 (2010).
[21] X.-L. Qi, T. L. Hughes, and S.-C. Zhang, Phys. Rev. B **82**, 184516 (2010).
[22] J. Röntynen and T. Ojanen, Phys. Rev. Lett. **114**, 236803 (2015).
[23] L. Fu and C. L. Kane, Phys. Rev. Lett. **102**, 216403 (2009).
[24] A. R. Akhmerov, J. Nilsson, and C. W. J. Beenakker, Phys. Rev. Lett. **102**, 216404 (2009).
[25] S. B. Chung, X.-L. Qi, J. Maciejko, and S.-C. Zhang, Phys. Rev. B **83**, 100512 (2011).
[26] C.-X. Liu and B. Trauzettel, Phys. Rev. B **83**, 220510 (2011).
[27] G. Strübi, W. Belzig, M.-S. Choi, and C. Bruder, Phys. Rev. Lett. **107**, 136403 (2011).
[28] J. Wang, Q. Zhou, B. Lian, and S.-C. Zhang, Phys. Rev. B **92**, 064520 (2015).
[29] A. Yamakage and M. Sato, Physica E **55**, 13 (2014).
[30] J. J. He, J. Wu, T.-P. Choy, X.-J. Liu, Y. Tanaka, and K. T. Law, Nat. Commun. **5**, 3232 (2014).
[31] See Supplemental Online Material.
[32] G. E. Blonder, M. Tinkham, and T. M. Klapwijk, Phys. Rev. B **25**, 4515 (1982).
[33] O. Entin-Wohlman, Y. Imry, and A. Aharony, Phys. Rev. B **78**, 224510 (2008).
[34] Here we assume a perfect transmission between the NSC and the metallic wire attached to lead 3. If not, one would effectively have $t = 1 - r = 2\alpha R_A$ with $0 < \alpha < 1$.
[35] A. Gendiar, R. Krcmar, and T. Nishino, Prog. Theor. Phys. **122**, 953 (2009).
[36] C. Hotta and N. Shibata, Phys. Rev. B **86**, 041108 (2012).
[37] It does not affect the conductances whether a voltage lead is superconducting or metallic, since no current flows out of the lead.
[38] For type II SCs $B_c \approx \sqrt{B_{c1}B_{c2}}$, where B_{c1} and B_{c2} are the lower and upper critical fields.
[39] E. M. Lifshitz and L. P. Pitaevskii, *Statistical Physics Part 2: Theory of the Condensed State* (Pergamon Press, 1980) p. 182.